Published by
NIGERIAN SOCIETY OF PHYSICAL SCIENCES
Available online @ https://journal.nsps.org.ng/index.php/jnsps

J. Nig. Soc. Phys. Sci. 6 (2024) 2137

Journal of the Nigerian Society of Physical Sciences

Investigations on the structural, vibrational, optical and photocatalytic behavior of CuO, MnO and CuMnO nanomaterials

L. Guru Prasad[a,*], R. Ravikumar[b], R. Ganapathi Raman[c], R. Rajesh Kanna[d]

[a]*Department of Physics, Mangalore Institute of Technology & Engineering, Moodabidre, Mangalore, India*
[b]*Department of Physics, TKM College of Arts & Science, Karikode, Kollam, India*
[c]*Department of Physics, Saveetha Engineering College, Chennai, India*
[d]*Department of Electronics & Communication Engineering, M.Kumarasamy College of Engineering, Karur*

Abstract

CuO, MnO and CuMnO nanomaterials have been prepared using the chemical precipitation method. The structure of the nanomaterials has been confirmed using XRD analysis. Metal oxide vibrations have been identified and assigned to the vibrational band. The morphology of the prepared nanomaterials has been investigated in the SEM images. The optical band of the materials has been calculated using Tauc's relation from the UV-Vis spectrum. The photocatalytic nature of the prepared nanomaterials has been studied against Congo red and Malachite green dyes.

DOI:10.46481/jnsps.2024.2137

Keywords: Nanomaterials, UV-Vis analysis, Photocatalytic, Metal-oxides

Article History :
Received: 14 May 2024
Received in revised form: 03 July 2024
Accepted for publication: 18 July 2024
Published: 27 July 2024

Communicated by: B. J. Falaye

1. Introduction

Nowadays, dyes are the most relevant pollutants that cause water pollution. These dyes may create complications for the environment and when these dyes are discharged into water bodies, they may increase their toxicity.

The occurrence of dyes in water may block the photosynthesis process in the plants in the water bed and lead to problems in the aquatic system [1]. In addition, toxic carcinogenic products will be released due to dyes in the water bodies.

All the harmful effects of dyes are generally due to their complex aromatic structure [2]. Malachite green is a dye that leads to cancer, mutations, chromosomal disorders, and respiratory toxicity [3]. This dye must be handled cautiously, especially at appropriate concentrations and low temperatures. Congo red dye is a benzene-based dye. This causes allergic reactions and its decomposition results in carcinogenic products [4]. It creates irritation in the skin, eye and gastrointestinal. Congo red badly affects blood factors and clotting and induces drowsiness, leading to respiratory problems.

Therefore, it is important to remove or degrade the dyes in industrial waste. Protection of water sources from environmental contamination is one of the major issues. Several techniques have been adopted; nevertheless, each one has its limitations.

*Corresponding Author Tel. No.: +91-948-989-1251.
Email address: guruphysics@gmail.com (L. Guru Prasad)

In recent years, the application of electrochemical techniques in wastewater treatment has become increasingly important.

Conventional wastewater treatment technologies are mainly divided into three categories [5]. They are physical, chemical and biological. However, these methods often fail to achieve complete color removal, highlighting their ineffectiveness in treating certain pollutants. So, these conventional methods are ineffective. Mostly, these methods transfer the contaminants to another phase, creating a disposal problem. A wide area is required for biological treatment, and this method shows low flexibility in operation and design. Chemical methods need huge amounts of chemicals and they produce huge amounts of sludge, which requires treatment.

Numerous researchers have considered the photocatalytic method the most efficient and economical method to remove organic dye pollutants from the water [6]. Participation of nanomaterials in the photocatalysis process is an emerging and efficient method in green technology. Metal oxides nanoparticles are the promising photocatalysts to degrade the water pollutants [7]. Recently, there has been significant interest in developing multi-metal semiconducting composites and hybrid materials for photocatalytic applications using visible light. Efforts are particularly concentrated on designing mixed metal oxide semiconductor composites to improve their photocatalytic efficiency under visible light, with a special focus on purifying drinking water [8]. In this context, this manuscript reports on the preparation, characterization, and photocatalytic properties of CuO, MnO, and CuMnO nanomaterials against Congo red and Malachite green dyes.

2. Experimental details

2.1. Materials and methods

2.1.1. Synthesis of CuO nanoparticles

CuO nanoparticles were prepared using the chemical precipitation method by mixing a 0.1 M Copper nitrate solution with a 0.02 M Citric acid. Sodium hydroxide solution was prepared with a 0.5 M concentration and added drop-wise in the copper nitrate & citric acid mixer. While adding this, the bluish-green color of the solution turned into thick blue. The residue was allowed to settle by the action of gravity. This precipitation was washed in distilled water to remove the impurities further and annealed at 800 °C for two hrs.

2.1.2. Synthesis of MnO nanoparticle

Manganese Oxide was also prepared using the chemical precipitation method. A 0.1 M Manganese acetate and a 0.02 M citric acid solution were prepared in distilled water and mixed well. In this, mixer, a 0.5 M NaOH solution was added at a prolonged and steady rate. While adding NaOH, the solution's colour changed to brown precipitation. To get the pure sample, it was washed in distilled water and annealed at 800 °C for two hrs.

2.1.3. Synthesis of CuMnO nanocomposite

For preparing the nanocrystalline copper manganese oxide, a 0.1 M of Copper nitrate and Manganese acetate and a 0.02 M of Citric acid were prepared and mixed well. NaOH solution was slowly added into that mixer, which yielded the precipitation. As mentioned in the other sample preparation, a washing and annealing procedure was carried out to get a pure CuMnO sample.

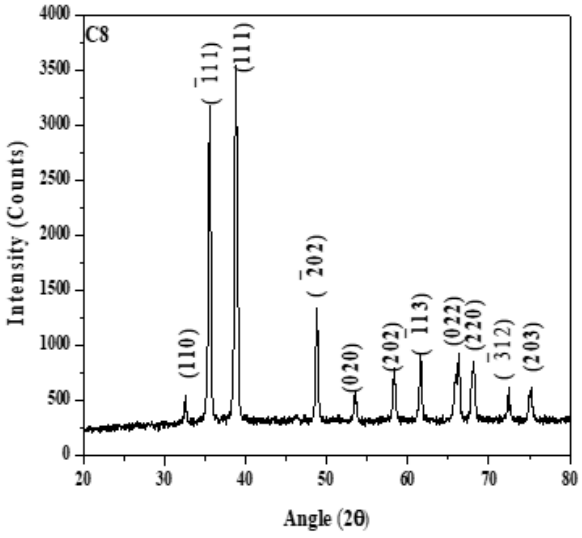

Figure 1. XRD pattern of CuO nanoparticle.

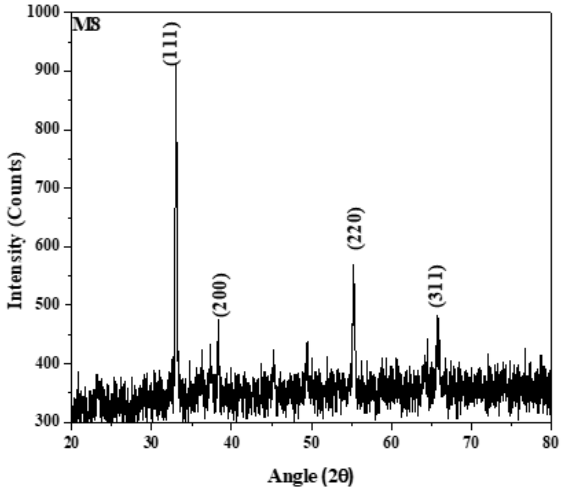

Figure 2. XRD pattern of MnO nanoparticle.

2.2. XRD analysis

The XRD analysis of the prepared nanoparticles and nanocomposite was carried out with the help of the XRD instrument XPERT-PRO model powder diffractometer having Cu-k

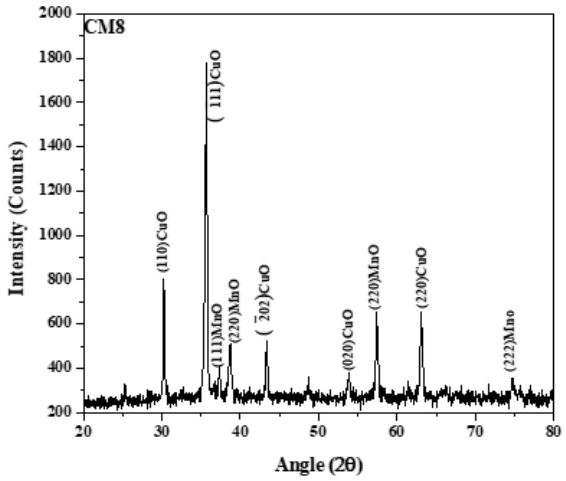

Figure 3. XRD pattern of CuMnO nanocomposite.

radiation (λ =1.54060A) operating at 40 kV, 30 mA. The pattern is recorded at 2Θ angle between 20° to 80°. Sherr's equation carries out the particle size determination and the β value corresponding to each peak is calculated by the Pseudo Voigt curve fit method. The corresponding curve fit is shown in Figure 1.

Well-distinguished peaks have been observed, confirming the prepared samples' crystallinity. The XRD pattern of the prepared sample is compared with the standard pattern (card no:801916) and confirms that the prepared CuO sample crystallizes in a monoclinic structure. Also, the average grain size of the prepared CuO is 18 nm. Figure 2 shows the XRD patterns of MnO nanoparticles. Well, distinguished sharp peaks are observed at (1 1 1), (2 0 0), (2 2 0), and (3 1 1) and it confirms the crystalline nature of the prepared MnO nanoparticles. The cubic crystal system of MnO is confirmed by comparing the recorded pattern with the standard JCPS file (card no:044-014) and it is found that the crystallite size of the prepared MnO is 28 nm. Figure 3 shows the XRD patterns of CuMnO confirming the good crystallinity nature of the prepared nanomaterial. Peaks observed at various angles were compared with the standard patterns of CuO and MnO (card no:801916 and 044-014) and the crystal grain size has also been obtained for the prepared nanomaterial and shown in Table 1.

The reduction in particle size of nanomaterials is known to improve degradation performance by increasing surface active sites. Conversely, it can also potentially decrease the degradation rate by promoting surface recombination of electrons and holes. preferential treatment.

2.3. Vibrational analysis

FTIR Analysis is used to define the different functional groups present in the prepared nanoparticles and nanocomposite. The obtained vibrational peaks are compared with the FTIR library and the existence of functional groups such as CO, OH, and metal oxide vibrational notes is found.

Table 1. The grain size of the CuO, MnO, and CuMnO particles.

Nanoparticle	2θ	Θ	Cos θ	B	T (nm)	Average (nm)
CuO	35.5	17.7	0.952	0.419	19.902	18.251
	38.70	19.3	0.943	0.520	16.192	
	48.8	24.4	0.910	0.467	18.660	
MnO	33.0	16.5	0.959	0.257	32.295	27.940
	55.2	27.6	0.886	0.318	28.248	
	65.8	32.9	0.839	0.407	23.276	
CuMnO	35.5	16.2	0.999	0.193	41.028	33.173
	35.6	17.8	0.952	0.268	31.150	
	57.4	28.7	0.877	0.331	27.342	

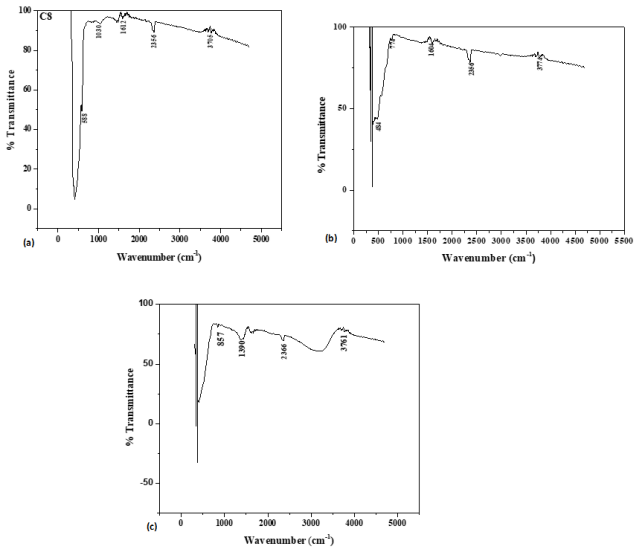

Figure 4. FTIR spectrum of (a) CuO nanoparticle (b) MnO nanoparticle and (c) CuMnO nanoparticle.

The FTIR spectrum of the CuO nanomaterials is shown in Figure 4a. Generally, due to the inter-atomic vibration of metal-oxide peaks, they may be observed below 1000 cm^{-1}. In the current investigation, this is observed at 1030 cm^{-1}. A sharp and broad peak observed at 535 cm^{-1} confirms the formation of the CuO bond and it is assigned to the Cu-O stretching vibration. Additionally, a peak was observed at 588 cm^{-1}. These two bands confirm the monoclinic phase of the prepared material [9].

The nanomaterials tend to absorb moisture since they have a high surface-to-volume ratio [10]. Due to this, a low absorption peak is observed at 3705 cm^{-1} which is assigned to OH stretching vibration.

FTIR spectrum of MnO is shown in Figure 4b. From Figure 4b it is noticed that the stretching vibration of the MnO vibrational band occurred at 484 cm^{-1}. The absorption band traced at 774 cm^{-1} raises due to metal oxide bond vibration. The vibrational bands observed at 1604 cm^{-1}, 2356 cm^{-1} and 3774 cm^{-1} represent O-H bending, Cu absorption bands and O-H stretching vibrations respectively.

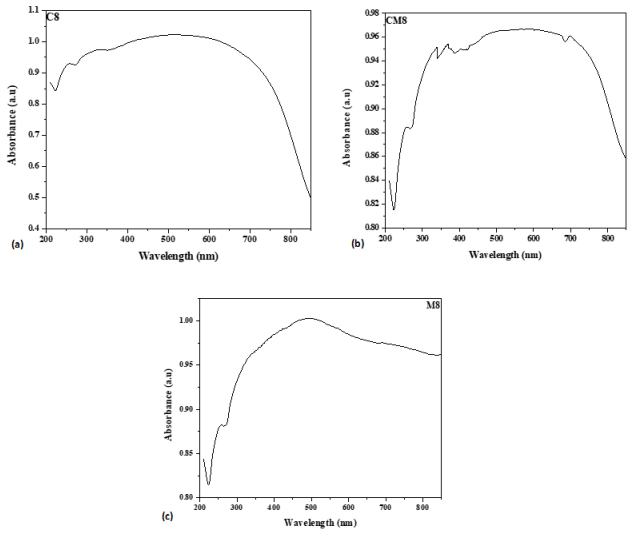

Figure 5. UV-Vis spectrum of (a) CuO nanoparticle (b) MnO nanoparticle and (c) CuMnO nanoparticle.

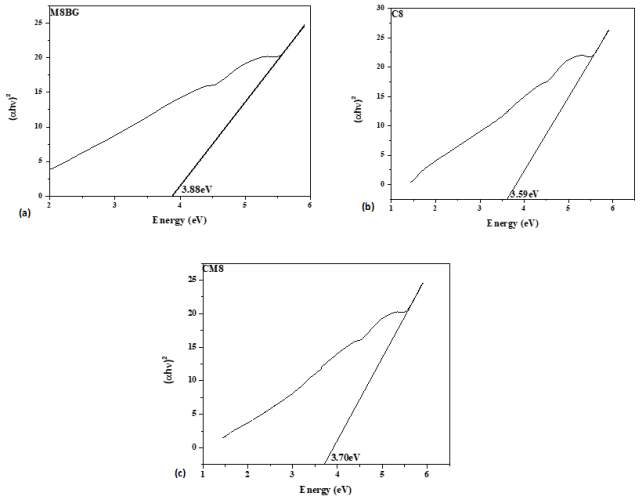

Figure 6. Tauc plot of (a) CuO (b) MnO and (c) CuMnO.

The recorded FTIR spectrum of CuMnO is presented in Figure 4c. It is noticed from Figure 4c, the major vibration of CuMnO occurs at 857 cm-1, 1390 cm^{-1}, 2366 cm^{-1} and 3761 cm^{-1}. The absorption peak visible at 857 cm^{-1} confirms the metal oxygen stretching vibration and 1390 cm^{-1} indicates the vibration peak of CuO. The Cu absorption band is assigned to the band observed at 2366 cm^{-1} and a vibrational peak experimentalized at 3761 cm^{-1} represents O-H stretching vibration.

2.4. *UV –Visible spectroscopy analysis*

Optical spectrum analysis is carried out with the help of a JASCOV650 UV/Vis spectrophotometer and the wavelength range is taken from 210 nm to 800 nm with a resolution of 1 nm. The optical bandgap of prepared nanoparticles and nanocomposite is found with the help of the Tauc relation.

It is visible from Figure 5 that the prepared nanomaterials have very low absorption in the visible region, which confirms the suitability of the materials for photonic applications. It is found in Figure 6. that CuO has a band gap at 3.59 eV, MnO at 3.88 and CuMnO of 3.70 eV. The photocatalytic behaviour strongly depends on the electronic structure and band gap. The band gap value of the prepared materials confirms the suitability of materials for photodegradation [11].

2.5. *SEM analysis*

Samples are analyzed through JEOL/EO Model JSM-6390LV Scanning electron microscope. It is used to analyze the surface morphology of prepared nanoparticles and nanocomposite. The SEM image (Figure 7a) of CuO nanoparticles shows that the particles are homogeneous in nature and spherical in shape. The agglomeration of particles is limited due to the use of a good stabilizer. The SEM image of MnO (Figure 7b) shows that the particles are highly agglomerated due to the Vander Wall force of attraction and particle. The overall shape of

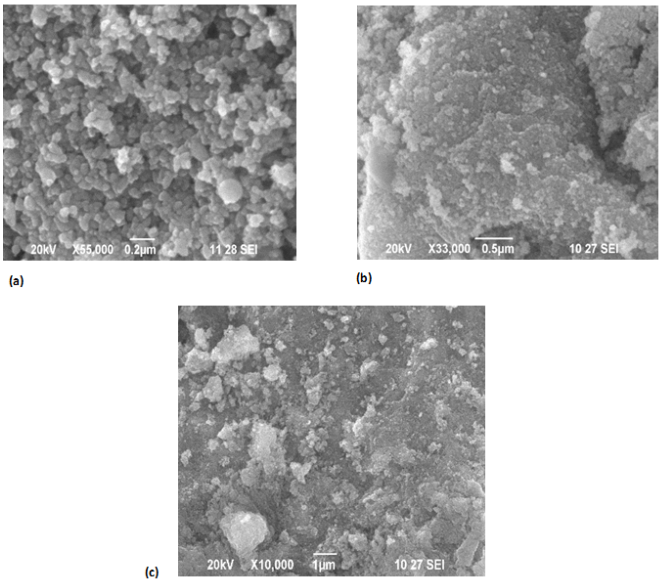

Figure 7. SEM image of (a) CuO (b) MnO and (c) CuMnO.

the MnO shows a sheet-like structure. It is confirmed from the SEM image (Figure 7c) that the CuMnO nanomaterial is well-defined and scattered in a plane. When the material is compared with MnO nanoparticles, the agglomeration is limited in the CUMnO sample due to the nanocomposite formation.

2.6. *Photocatalytic degradation studies of nanoparticles*

In the present study, the photocatalytic activity of CuO, MnO nanoparticles has been studied and compared with the activity of CuMnO nanomaterials. Here, we have taken the Congo red and Malachite green dyes and their degradation under UV light has been investigated. The photocatalytic cell was filled with dye solution and in that, 0.1 g of catalyst (prepared nano-

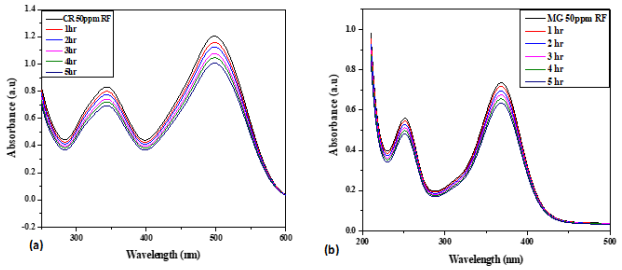

Figure 8. Photocatalytic degradation of (a) Congo red dye and (b) Malachite green using CuO nanoparticles.

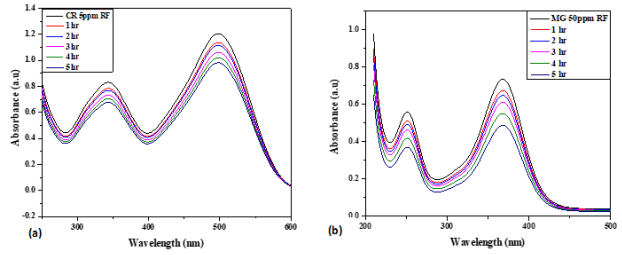

Figure 9. Photocatalytic degradation of (a) Congo red dye and (b) Malachite green using MnO nanoparticles.

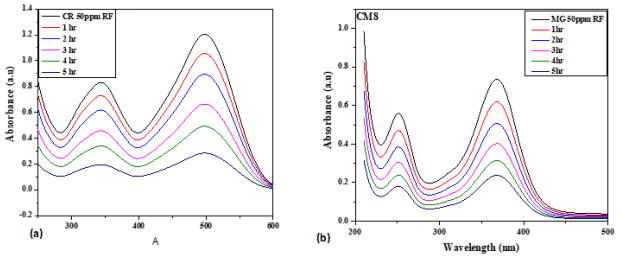

Figure 10. Photocatalytic degradation of (a) Congo red dye and (b) Malachite green using MnO nanoparticles.

material) was added. This was irradiated with UV light and the light absorption was measured. The absorption level is analyzed with the help of the UV-visible spectrum.

It is observed from Figure 8 that the Congo red dye absorption rate is about 1.2 initially and after 5 hr it turns to 0.8447 and for Malachite green, it is from 0.7357 to 0.5870.

It is observed from Figure 9 that the absorption rate of congo red is about 1.2 initially and after 5 hours it turns to 0.9120 and Malachite green, it drops from 0.7357 to 0.4854 after 5 hours.

Figure 10 shows that for Congo red, the absorption rate is about 1.2 initially and after 5 hr it turns to 0.2872. In the case of Malachite green initial absorption rate is 0.7357 after 5 hr, it turns to 0.2374 if the CuMnO is added.

It is visible that higher degradation occurs for CuMnO nanomaterials compared to CuO & MnO nanomaterials [12].

The synthesized CuO nanomaterials degrade 30% of Congo red dye in 5 hours, while MnO nanomaterials degrade only 24% in the same period. According to the literature, Cu-loaded catalysts are effective for photodegradation. Arora *et al.* [13] reported a 60% degradation of Congo red using Cu-loaded Fe_3O_4@TiO_2. In contrast, in the present study, CuMnO nanomaterials achieve nearly 75% degradation of Congo red dye within 5 hours.

Similarly, CuO and MnO nanomaterials reduce Malachite green dye by 20% and 35%, respectively, in 5 hours, but CuMnO nanomaterials degrade around 70% of Malachite green dye in the same duration. The increased degradation rate is due to the reduced recombination rate of charge carriers.

The band gap of a semiconducting photocatalyst is a key factor in determining its degradation efficiency [14]. Typically, a lower band gap enhances photocatalytic activity. In this study, both CuO has band gap of 3.59 eV, while the CuMnO material has a slightly higher band gap of 3.70 eV. Despite the higher band gap, CuMnO exhibits superior photocatalytic degradation performance. Literature studies indicate that hybrid copper-manganese oxides exhibit a high amount of oxygen vacancies due to strong charge transfer, which enhances their degradation performance [15]. Given that Cu and Mn are non-toxic, the current studies suggest that CuMnO materials are effective photocatalytic agents for removing both Congo red and Malachite green dyes from water.

3. Conclusion

In the present study, CuO nanoparticles, MnO nanoparticles, and CuMnO nanoparticles were prepared by the chemical precipitation method using copper nitrate, manganese acetate, sodium hydroxide and citric acid. From XRD, it was revealed that CuO nanoparticles show a crystalline nature and monoclinic structure, having an average particle size of about 18 nm and MnO crystallizes in a cubic structure with a particle size of about 28 nm and CuMnO nanocomposite has an average particle size of about 33 nm. The function group and its vibrational nature have been identified in FTIR analysis. The suitability of the materials for the photocatalytic activity has been recognized from the band gap analysis. Compared to CuO and MnO, CuMnO nanomaterials exhibit superior photocatalytic performance against Congo red and Malachite green, confirming their suitability for water purification applications.

References

[1] R. Al-Tohamy, S. S. Ali, F. Li, K. M. Okasha, Y. A.-G. Mahmoud, T. Elsamahy, H. Jiao, Y. Fu & J. Sun, "A critical review on the treatment of dye-containing wastewater: Ecotoxicological and health concerns of textile dyes and possible remediation approaches for environmental safety", Ecotoxicology and Environmental Safety **231** (2022) 113160. https://doi.org/10.1016/j.ecoenv.2021.113160.

[2] B. Lellis, C. Z. Fávaro-Polonio, J. A. Pamphile & J. C. Polonio, "Effects of textile dyes on health and the environment and bioremediation potential of living organisms", Biotechnology Research and Innovation **3** (2019) 275. https://doi.org/10.1016/j.biori.2019.09.001.

[3] S. Srivastava, R. Sinha & D. Roy, "Toxicological effects of malachite green", Aquatic Toxicology **66** (2004) 319. https://doi.org/10.1016/j.aquatox.2003.09.008.

[4] S. I. Siddiqui, E. S. Allehyani, S. A. Al-Harbi, Z. Hasan, M. A. Abomuti, H. K. Rajor & S. Oh, "Investigation of congo red toxicity towards different living organisms: A Review", Processes **11** (2023) 807. https://doi.org/10.3390/pr11030807.

[5] E. K. Shah & V. Gandhi, "Advances in wastewater treatment 1", Materials Research Foundations **91** (2021) 1. https://doi.org/10.21741/9781644901144-1.

[6] M. A. Al-Nuaim, A. A. Alwasiti & Z. Y. Shnain, "The photocatalytic process in the treatment of polluted water", Chemical Papers **77** (2023) 677. https://doi.org/10.1007/s11696-022-02468-7

[7] M. S. S. Danish, L. L. Estrella, I. M. A. Alemaida, A. Lisin, N. Moiseev, M. Ahmadi, M. Nazari, M. Wali, H. Zaheb & T. Senjyu, "Photocatalytic applications of metal oxides for sustainable environmental remediation", Metals **11** (2021) 80. https://doi.org/10.3390/met11010080.

[8] A. Rahman, H. Sabeeh, S. Zulfiqar, P. O. Agboola, I. Shakir & M. F. Warsi, "Structural, optical and photocatalytic studies of trimetallic oxides nanostructures prepared via wet chemical approach", Synthetic metals **259** (2020) 116228. https://doi.org/10.1016/j.synthmet.2019.116228.

[9] I. Z. Luna, L. N. Hilary, A. M. S. Chowdhury, M. A. Gafur, N. Khan & R. A. Khan, "Preparation and characterization of Copper Oxide nanoparticles synthesized via chemical precipitation method", Open Access Library Journal **2** (2015) 1. http://dx.doi.org/10.4236/oalib.1101409.

[10] A. Radhakrishnan & B. B. Beena, "Structural and optical absorption analysis of CuO nanoparticles", Indian Journal of Advances in Chemical Science **2** (2014) 158. https://api.semanticscholar.org/CorpusID:36219452.

[11] M. B. Tahir, M. Sohaib & M. Sagir, "Role of Nanotechnology in Photocatalysis", Encyclopedia of Smart Materials **2** (2002) 578. https://doi.org/10.1016%2FB978-0-12-815732-9.00006-1.

[12] I. Groeneveld, M. Kanelli, F. Ariese & M. R. van Bommel, "Parameters that affect the photodegradation of dyes and pigments in solution and on substrate – an overview", Dyes and Pigments **210** (2023) 110999. https://doi.org/10.1016/j.dyepig.2022.110999.

[13] P. Arora, A. Fermah, J. K. Rajput, H. Singh & J. Badhan "Efficient solar light-driven degradation of Congo red with novel Cu-loaded Fe_3O_4@TiO_2 nanoparticles", Environment Science and Pollution Research **24** (2017) 19546. https://doi.org/10.1007/s11356-017-9571-7.

[14] M. Khatun, P. Mitra & S. Mukherjee, "Effect of band gap and particle size on photocatalytic degradation of NiSnO3 nanopowder for some conventional organic dyes", Hybrid Advances **4** (2023) 100079. https://doi.org/10.1016/j.hybadv.2023.100079.

[15] J. Bao, X. Duan & P. Zhang, "Facile synthesis of a CuMnOx catalyst based on a mechanochemical redox process for efficient and stable CO oxidation", Journal of Material Chemistry A **46** (2020) 24438. https://doi.org/10.1039/D0TA07304K.